Deposition and characteristics of bismuth sulfide thin films by an in situ chemical reaction process at room temperature: a facile and eco-friendly approach

Weiyan Liu · Huiming Ji · Jian Wang · Xuerong Zheng ·
Junyun Lai · Junna Ji · Tongfei Li · Yuanliang Ma ·
Haiqin Li · Suqin Zhao · Zhengguo Jin

Abstract Uniform, smooth and densely packed Bi_2S_3 thin films were prepared at room temperature by an in situ solution chemical reaction using bismuth nitrate as precursor in a form of thin solid film which was reacted with ammonium sulfide ethanol solution. Bi_2S_3 thin films both as-deposited and annealed at different temperatures were characterized by XRD, SEM, EDS, AFM, UV–Vis–NIR and LSV measurements. The thin films growth with deposition cycle numbers was investigated. The results showed that the as-deposited Bi_2S_3 thin films were almost amorphous and near to chemical stoichiometry. The annealing promoted crystallization to orthorhombic structure as well as crystal growth from very small particles to short-rod shaped nanocrystals. The optical band-gap energy was in the range of 1.34–1.69 eV depended on crystal size on films. The eight dip-cycles Bi_2S_3 films annealed at 300 °C had a better photoelectrochemical performance with photocurrent density of 5.03 mA/cm^2 bias 0.5 V vs. Ag/AgCl reference electrode. This in situ deposition had an average deposited rate of 40 nm per cycle and a self-perfect function to grow smooth with increase of dip-cycle numbers.

W. Liu · H. Ji · J. Wang · X. Zheng · J. Lai · J. Ji · T. Li ·
Z. Jin (✉)
School of Materials Science and Engineering, Key Laboratory
for Advanced Ceramics and Machining Technology of Ministry
of Education, Tianjin University, Tianjin 300072, People's
Republic of China
e-mail: zhgjin@tju.edu.cn; zhgjin_tju@126.com

Y. Ma · H. Li · S. Zhao
College of Physics and Electronic Information Engineering,
Qinghai University for Nationalities, Xining 810007, People's
Republic of China

1 Introduction

In the past few years, semiconductor nanomaterials have been focus of scientific research due to their potential applications as active absorbers in photovoltaic, thermoelectric, photoelectro-chemical and sensing techniques [1–4]. For this purpose, many research works have been directed toward synthesis of semiconducting nanomaterials through comparatively facile, low cost and eco-friendly methods, in which solution chemical methods have shown great promise in high feasibility, low energy consumption and large-scale preparation [5, 6].

Bismuth sulfide, as a metal chalcogenide compound, has varied and unique semiconductor properties, such as direct band gap energy of 1.2–1.7 eV [7–9], high absorption coefficient of 10^{-4} cm^{-1} in the visible wavelength range [10], low-toxicity [11] and good chemical stability [12]. All these have been related to its potential applications in visible-wavelength photodetectors [13, 14], photoelectro-chemical solar cells [15, 16], thermoelectric devices [17, 18] and electrochemical hydrogen storage [19, 20]. Particularly, Bi_2S_3, as n-type semiconductor sensitizer, had been used in the sensitized oxide nanocrystalline photoelectrochemical cells (NPC) [14, 21, 22]. However, the previous studies showed that relatively low photoelectric conversion efficiency, typically less than 1 %, needed to be improved. So, new film preparation methods for uniform deposition of sensitizer layer on the oxide anodes and close contact at interface layers is still desired [23, 24].

Up to now, Bi_2S_3 thin films have been deposited by various solution chemical methods, mainly including chemical bath deposition (CBD) [25, 26], successive ion layer adsorption and reaction method (SILAR) [27, 28], electrochemical method [29, 30] and spray pyrolysis [31, 32]. CBD is a common solution chemical growth technique

for many metal chalcogenide compounds [33–35], which is, generally, easy to prepare thin films with high quality. However, it is known that in a CBD process, a heterogeneous growth of thin films on the substrate surface and a homogeneous growth of precipitates in the bulk solution took place simultaneously as the ionic product (IP) exceeded the solubility product (SP) in the CBD solution. The homogeneous growth of precipitates in the bulk solution was useless to thin film growth and only led to loss of the precursor sources and then additional environmental pollution [36] In addition, there is an up-limit on film thickness, which means there is no significant increase in film thickness even by longer deposition time due to the equilibrium of adsorption growth and desorption dissolution [37]. SILAR deposition is a solution growth technique based on alternate immersion of a deposited substrate into separate cationic and anionic precursor solutions. It only utilized synthetic reaction of the ion-absorbed layers on the deposited substrate to grow thin films by layer by layer deposition cycles repeatedly. The loss of precursor sources is lower when compared with that of CBD process. Several SILAR methods had been used to grow Bi_2S_3 thin films. The studies reported showed that high quality of the deposited thin films is still desired by SILAR process [27, 38]. In addition, relatively low deposition rate of SILAR process, typically about 0.34 nm/cycle [38], is a disadvantage for high time-efficiency process.

Recently, an in situ solution chemical reaction deposition had been suggested by our laboratory for preparation of CdS thin films [36, 39, 40]. Here, we developed the new deposition method to deposit Bi_2S_3 thin films. It used separate cationic and anionic precursor solutions similarly as SILAR but the deposition reaction took place on cationic precursor solid films instead of the ion-absorbed layers. The deposited Bi_2S_3 thin films had an average growth rate of 40 nm per deposition cycle, far higher than that of SILAR method. The thin film samples including the as-deposited and annealed were characterized by XRD, FE-SEM, EDS, AFM, UV–Vis–NIR and LSV measurements. The thin film growth with deposition cycle numbers was investigated.

2 Experimental

2.1 Chemicals

For the in situ solution chemical deposition of Bi_2S_3 thin films, the following chemicals were used: bismuth nitrate [$Bi(NO_3)_3\cdot5H_2O$; 99.5 %], ammonium sulfide (($NH_4)_2S$; 40–48 %), ethylene glycol monomethylether ($C_3H_8O_2$; EGME; 99.0 %) and 1-butanol ($C_4H_{10}O$; 99.5 %), absolute ethanol (C_2H_6O; 99.7 %). All chemicals were purchased commercially and were directly used as received.

2.2 In situ solution chemical deposition

In situ solution chemical reaction process for preparing Bi_2S_3 thin films is shown in Fig. 1. Cationic solution for the pre-formed Bi^{3+} precursor films: an amount of

Fig. 1 Flow chart of deposition of Bi_2S_3 thin films by in situ solution chemical process
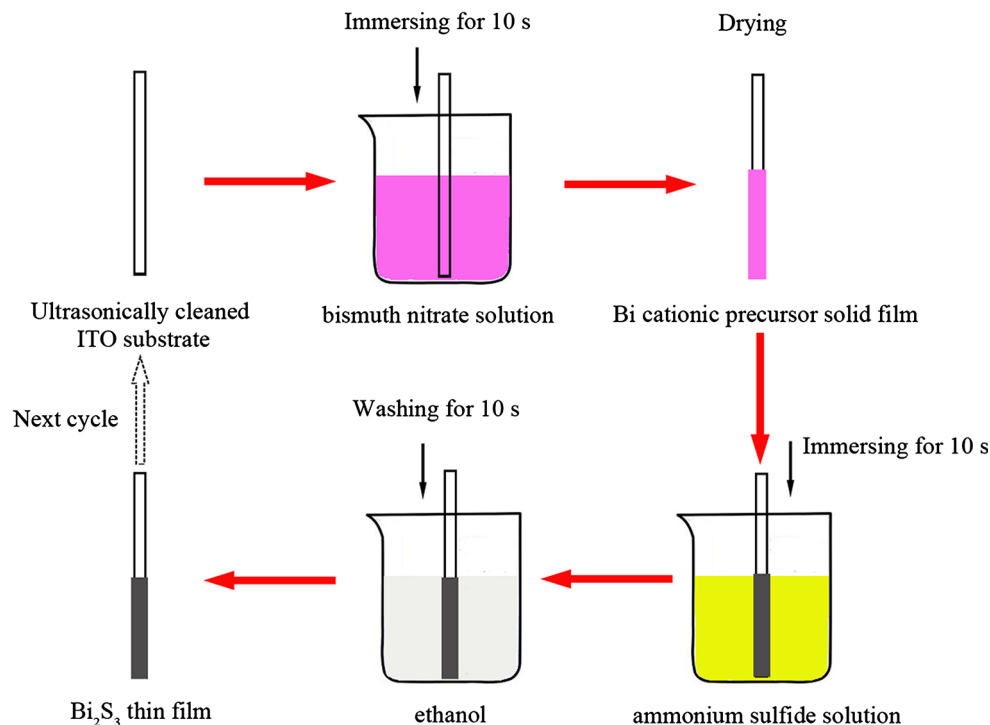
Bi(NO₃)₃·5H₂O was dissolved into a mixed solvent containing 9 ml EGME, 1 ml butanol at room temperature to gain 0.15 M Bi^{3+} precursor solution. Sulfur anionic reaction solutions: An amount of $(NH_4)_2S$ was dissolved into 10 ml ethanol at room temperature to gain 0.21 M $(NH_4)_2S$ solution. The ITO glass slides, as deposited substrates, were ultrasonically cleaned with acetone, deionized water, and absolute alcohol in sequence for the following deposition. One cycle of the in situ solution chemical reaction deposition contained three steps, as shown in Fig. 1a the cleaned ITO substrates were immersed into the Bi(NO₃)₃ EGME/butanol solution at room temperature for 10 s and then the Bi^{3+}-coated substrates were dried in an oven at 80 °C for 5 min. (b) the dried substrates with the preformed Bi precursor films were immersed into the $(NH_4)_2S$ ethanol solution for 10 s, where Bi^{3+} reacted with S^{2-} to form Bi_2S_3. (c) the as-deposited substrates were washed with ethanol to remove soluble ions. The one-cycle operation above was repeated to obtain certain film thickness. The as-deposited films were annealed at temperatures of 200, 300 and 400 °C for 30 min in argon atmosphere, respectively. The processing condition used in the experiment is listed in Table 1. The chemical reaction formulae involved in the in situ reaction process are given as follows:

$$Bi(NO_3)_3 \rightarrow Bi^{3+} + 3NO_3^{2-} \tag{1}$$

$$(NH_4)_2S \rightarrow 2NH_4^+ + S^{2-} \tag{2}$$

$$2Bi^{3+} + 3S^{2-} \rightarrow Bi_2S_3 \tag{3}$$

2.3 Characterization

The crystalline structure of the as-deposited and annealed Bi_2S_3 thin films were analyzed by X-ray diffraction (XRD, D8 advanced, Bruker, German) with CuKα radiation (λ = 1.54178 Å) at a scanning rate of 8°/min ranging from 2θ = 10°–70°. Surface morphology and cross-section of the films was observed by field emission scanning electron microscope (FE-SEM, S-4800, Hitachi, Japan). Chemical constituent of Bi_2S_3 thin film was detected by energy dispersive X-Ray fluorescence (EDX) attached TEM (JEM-2100F, JEOL, Japan). Three points on each film surface were selected to probe the chemical constituents of the films, and the given atomic percentage of element Bi and S was the average value of the three measured points.

Table 1 Processing condition for deposition of Bi_2S_3 thin films

Parameters	Cationic precursor (mol/L)	Anionic precursor (mol/L)
Sources	Bi(NO₃)₃	(NH₄)₂S
Volume of EGME (ml)	9	–
Volume of 1-butanol (ml)	1	–
Concentration (M)	0.15	0.21
Immersion time (s)	10	10
Immersion cycles (n)	2/4/6/8	2/4/6/8
Annealing temperature (°C)	200/300/400	200/300/400

Fig. 2 **a** Plan and cross-section FESEM morphologies of 6-cycle deposited Bi_2S_3 thin film, **b** XRD patterns of (1) bare ITO glass, (2) the 20-cycle deposited Bi_2S_3 thin film, **c** SAED pattern and **d** EDX spectrum of 6-cycle deposited Bi_2S_3 thin film
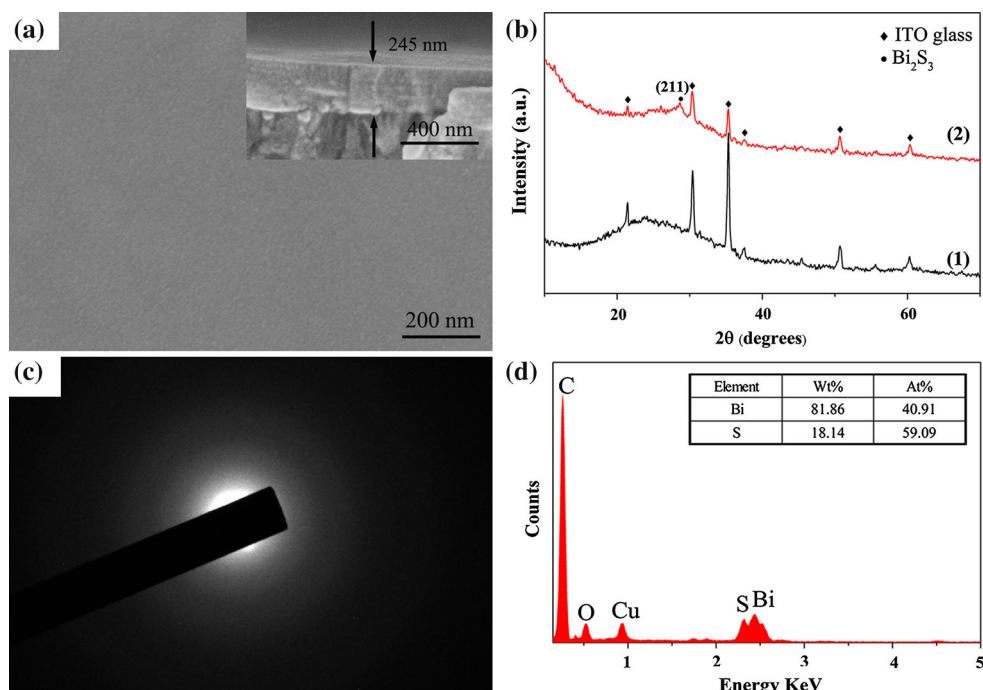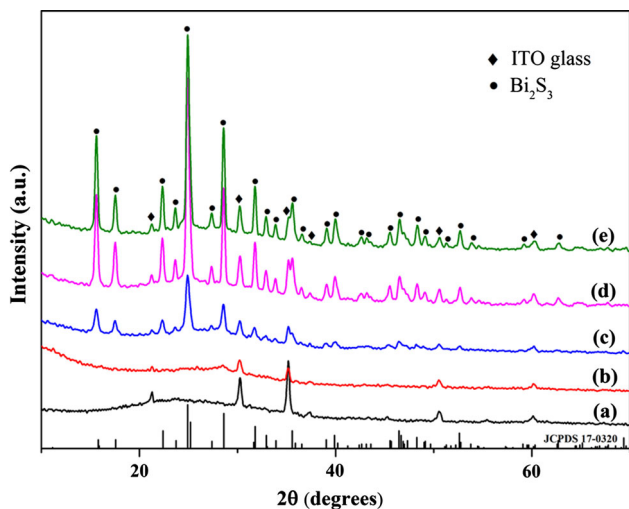
Fig. 3 XRD patterns of *a* bare ITO glass, and the 20-cycle deposited Bi_2S_3 thin films: *b* as-deposited, *c* annealed at 200 °C, *d* annealed at 300 °C and *e* annealed at 400 °C

Surface roughness and film thickness was characterized by a multimode nano scope IV atomic force microscope (AFM, 5500, Agilent, America). UV–vis–NIR spectra of the films at wavelength from 400 to 1,200 nm were collected with a UV–vis–NIR spectrophotometer (UV-3600, shimadzu, Japan). The linear sweep voltammetry characteristics of the samples were measured in a three-electrode photoelectrochemical cell (PEC) under dark and light illumination with AM 1.5, using a computer-controlled potentiostat (versaSTAT 3, Princeton Applied Research, America).

3 Results and discussion

3.1 As-deposited Bi_2S_3 thin films

Figure 2a shows plan and cross-section FESEM morphologies of the Bi_2S_3 thin films prepared with six dip-cycles at

Table 2 Structural parameters of Bi_2S_3 thin films calculated by XRD analyses

Annealing temperature (°C)	Average crystal size (nm)	Calculated lattice constants (Å)			Dislocation density δ (lines/m^2)
		Standard values			
		a = 11.149	b = 11.304	c = 3.981	
As-deposited	12.8	–	–	–	6.10×10^{15}
200	25.4	11.141	11.289	3.984	1.55×10^{15}
300	37.1	11.137	11.258	3.969	0.73×10^{15}
400	38.5	11.127	11.263	3.969	0.67×10^{15}

Fig. 4 FESEM plan views of 6-cycle deposited Bi_2S_3 films annealed at **a** 200 °C, **b** 300 °C, **c** 400 °C and **d** EDS spectrum of films annealed at 300 °C

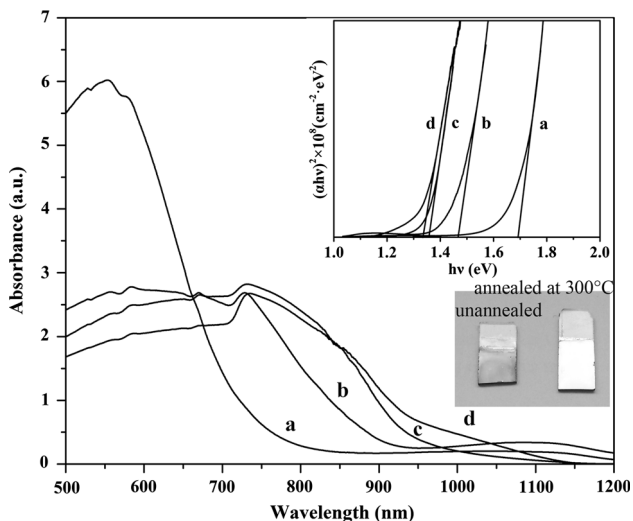| Element	Wt%	At%
Bi	81.86	40.91
S	18.14	59.09
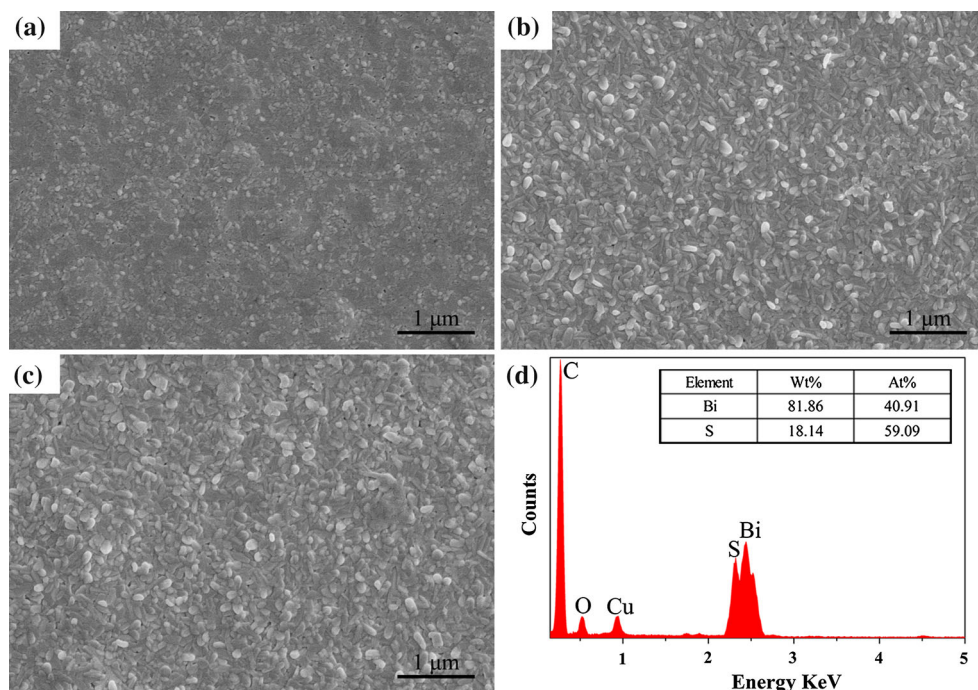
Fig. 5 Optical absorption spectra of the 6-cycle Bi_2S_3 thin films of *a* as-deposited, *b* annealed at 200 °C, *c* annealed at 300 °C and *d* annealed at 400 °C in Ar, and the *insets* are corresponding $(\alpha h v)^2$– *hv* curves and samples pictures

room temperature. It is seen that the as-deposited film is much smooth and the deposited particles on thin film are so small that they could not be seen clearly by high amplification SEM picture. The film thickness calculated by the cross-section image is about 245 nm. Figure 2b is XRD pattern of the as-deposited thin films with 20 dip-cycles,

showing only a weak characteristic diffraction peak at 28.6° which can be indexed to plane (211) of orthorhombic Bi_2S_3 (JCPDS 17-0320) except of the diffraction peaks of ITO glass. The SAED pattern also verifies that the as-deposited thin film has non-crystalline electronic diffraction characteristics (Fig. 2c). Both results indicate that the as-deposited thin film is almost of amorphous phase. Energy dispersive X-Ray fluorescence spectrum is shown in Fig. 2d. The Bi:S atomic ratio is 40.88:59.12, slightly Bi-rich compared with Bi_2S_3 chemical stoichiometry. In addition, elements C, O and Cu were also detected by EDX. Cu and C are mainly from the copper grid, and O is due to exposure to the atmosphere.

3.2 Annealed Bi_2S_3 thin films

The 6 cycle deposited Bi_2S_3 thin films were annealed in argon atmosphere at different temperatures. Figure 3 is XRD patterns of the Bi_2S_3 films as-deposited and annealed at 200 300and 400 °C, respectively. The standard diffraction pattern of JCPDS 17-0320 for orthorhombic Bi_2S_3 is also shown in Fig. 3. It is seen that characteristic diffraction peaks of orthorhombic Bi_2S_3 have appeared after annealing at 200 °C. These diffraction peaks become strong and sharp after annealing 300 and 400 °C. Furthermore, crystallite size calculated by the Scherrer's relation using plane (211) broadening, lattice constants and dislocation density by

Fig. 6 Dark and light current–voltage characteristics of Bi_2S_3 thin films (**a**) as-deposited, **b** annealed at 200 °C, **c** annealed at 300 °C and **d** annealed at 400 °C
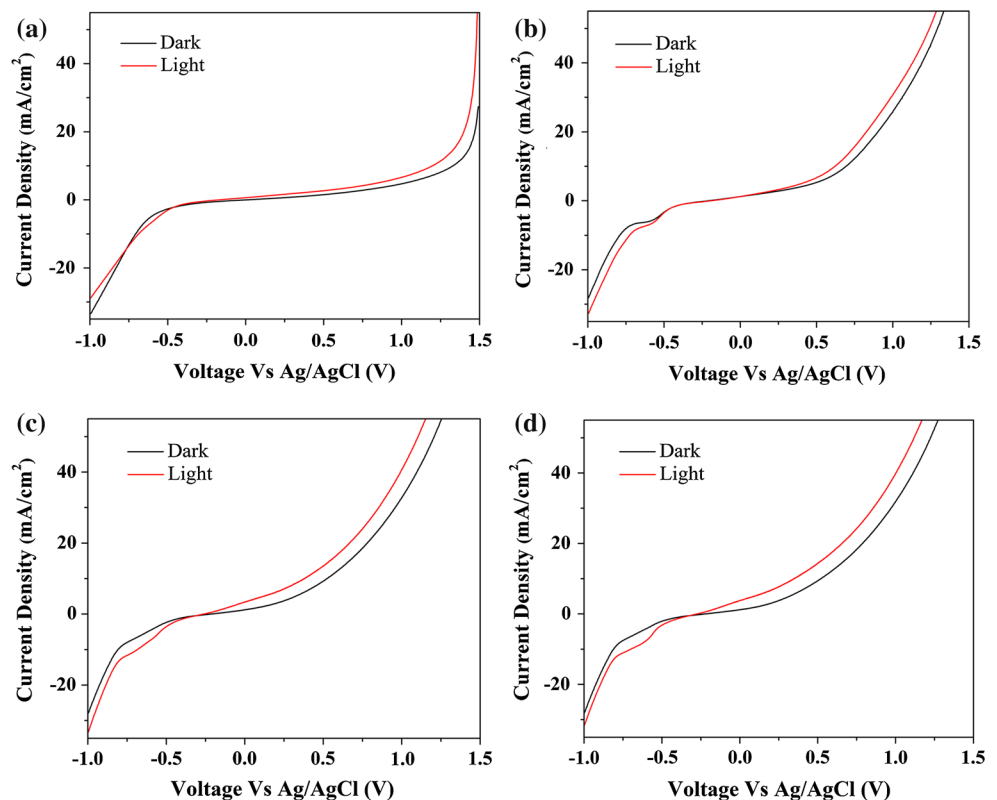
XRD analysis are listed Table 2. It is seen that the crystallite size calculated is 12.8, 25.4, 37.1 and 38.5 nm, respectively, for the as-deposited Bi_2S_3 thin films and those annealed at 200, 300 and 400 °C. The lattice constants calculated are well agreement with the standard values of orthorhombic Bi_2S_3 structure. The dislocation density is decreased with increasing annealing temperature. All these XRD analyses indicate that the low temperature annealing in Ar atmosphere promote crystallization and crystal growth of the as-deposited Bi_2S_3 thin films.

Figure 4a–c show FESEM images of the annealed Bi_2S_3 thin films. It is seen that the annealed Bi_2S_3 thin films are still uniform, smooth and densely packed. With increase of annealing temperature, the deposited crystallites grew gradually into irregularly short-rod shaped morphology and crystal size became large, which should be attributed to secondary crystal growth induced by annealing. Figure 4d is EDS spectrum of the Bi_2S_3 thin films annealed at 300 °C. The Bi:S atomic ratio is 40.91:59.09, still slightly Bi-rich similarly to that of the as-deposited Bi_2S_3 thin films. The result indicates that the annealing in argon atmosphere changed the deposited morphology and crystal size but not chemical constituent of Bi_2S_3 thin films.

Figure 5 shows absorption spectra of the as-deposited and annealed Bi_2S_3 thin films at different temperatures. It is seen that the as-deposited Bi_2S_3 thin film has special absorption spectrum which is different from that of the annealed thin films. It shows an enhanced absorption started about at 850 nm and an absorption peak at 550 nm in wavelength. The annealed thin films at 300 and 400 °C show slow shoulder absorption started at 1,150 nm and then enhanced successively toward high and broad absorption in the visible light region. The annealed thin film at 200 °C shows a transitional feature of absorption between both above. The band gap energies were evaluated by the Tauc' equation based on direct band-gap Bi_2S_3:

$$(\alpha h v)^2 = \kappa \left(h v - E_g \right) \qquad (4)$$

Fig. 7 Plan and cross-section FESEM morphologies of Bi_2S_3 thin films with deposition cycle numbers of a 2, b 4, c 6 and d 8, and then annealed at 300 °C, e film thickness versus cycle number as determined by FESEM
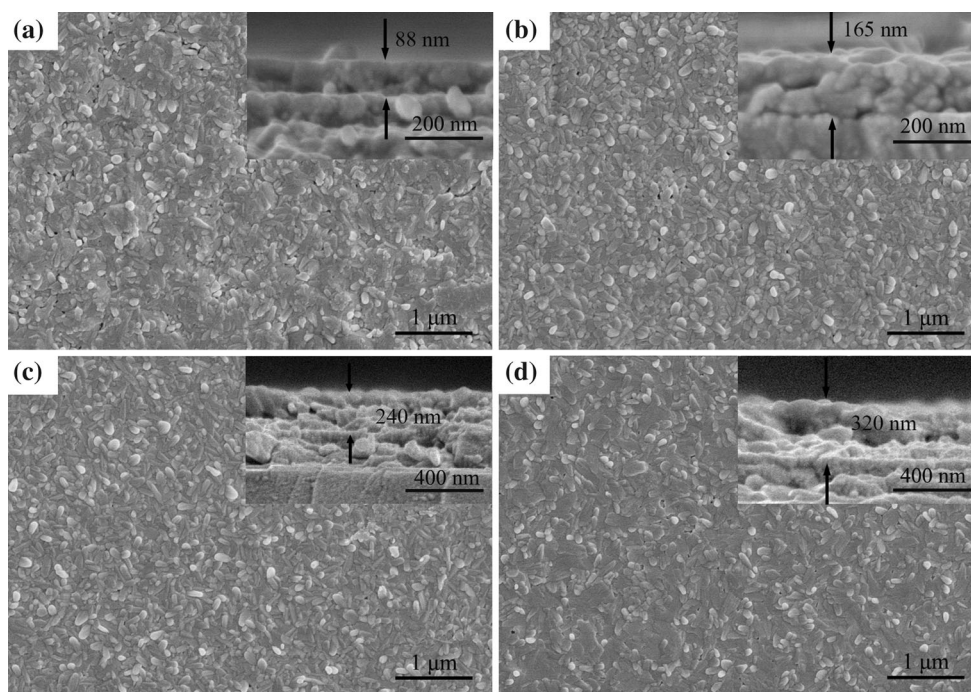
Fig. 8 Plan view and cross-sectional AFM images of Bi$_2$S$_3$ thin films deposited with different cycles **a**, **a'** 2, **b**, **b'** 4, **c**, **c'** 6, and **d**, **d'** 8, the *horizontal lines* in the plan view images are scanning traces
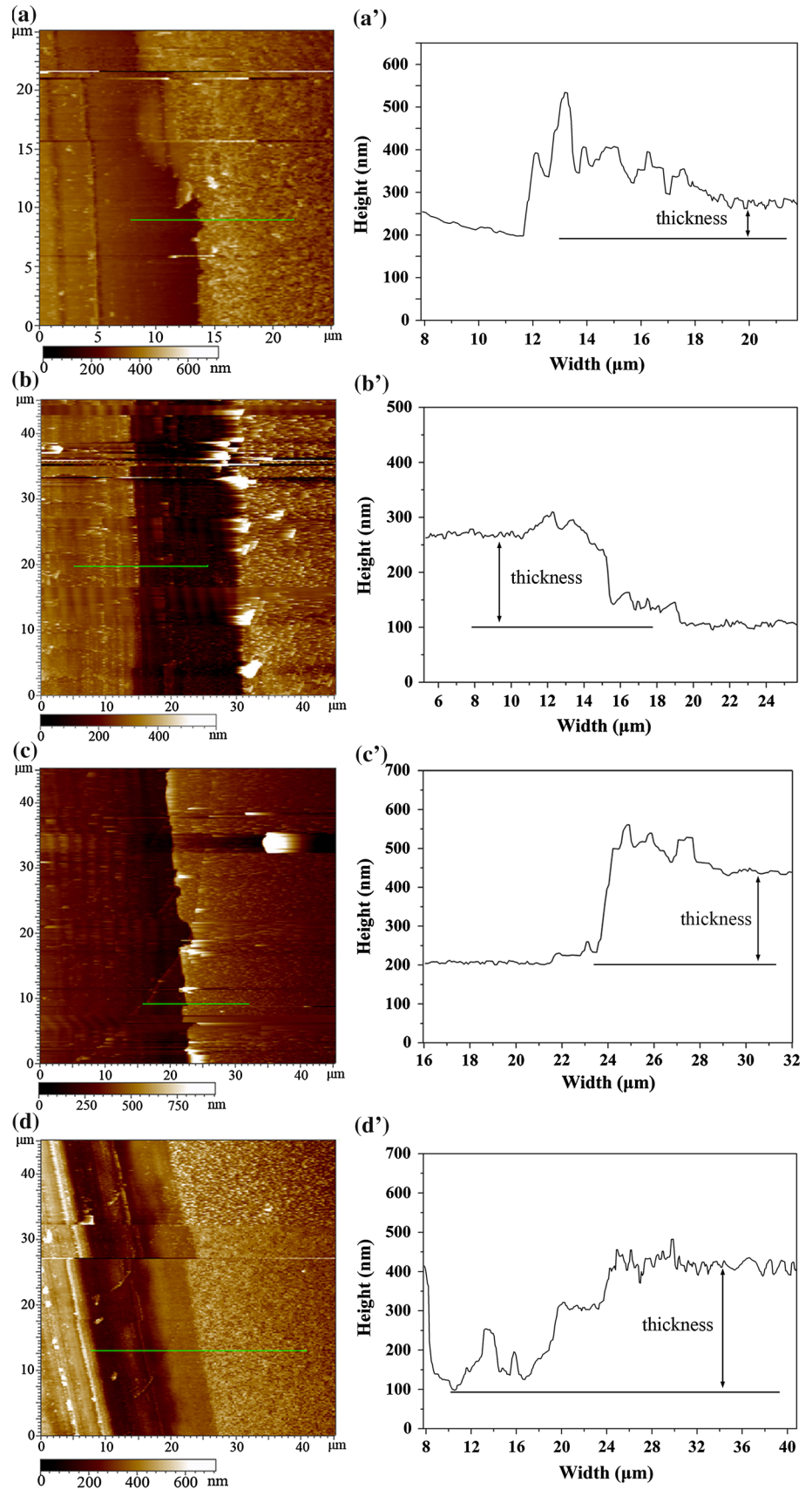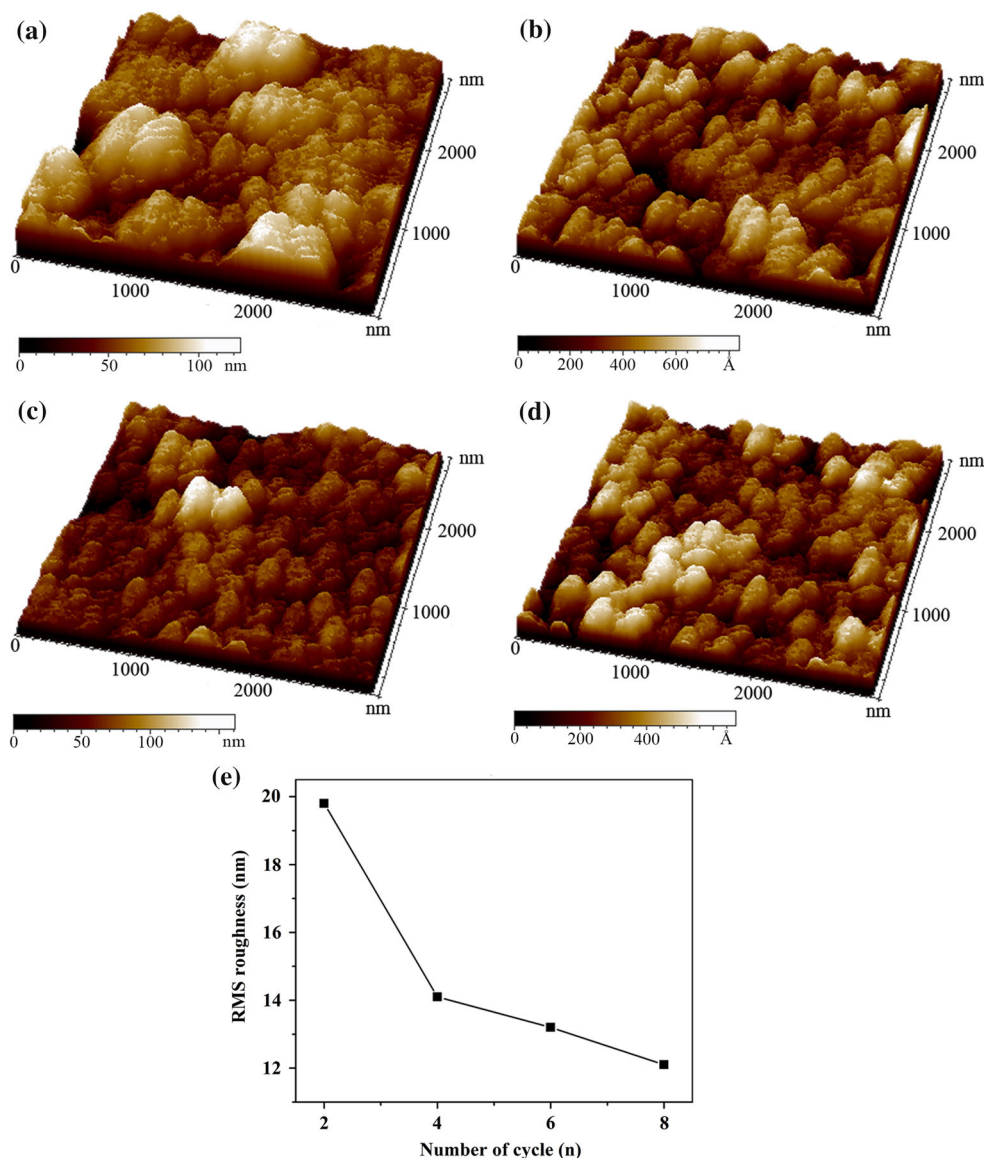
Fig. 9 Three-dimensional AFM images of Bi_2S_3 thin films with deposition cycle numbers of **a** 2, **b** 4, **c** 6 and **d** 8 and then annealed at 300 °C, and **e** film roughness versus cycle numbers determined by AFM

where κ is optical transition dependent constant, E_g is optical energy band gap, v is frequency of incident beam, h is Planck's constant. The plot of $(\alpha h v)^2$ versus hv is shown in the inset of Fig. 5. The calculated values are 1.69, 1.47, 1.36 and 1.34 eV, respectively, for the as-deposited thin film and those annealed at 200, 300 and 400 °C, which lie within the reported values [13, 41, 42]. The decrease of band gap with increase of annealing temperature is well consisted with the red shift of absorption spectra of Bi_2S_3 thin films. It is directly associated with crystal growth to large crystal size by annealing as well as increase of annealing temperature. So, it could be concluded that the as-deposited Bi_2S_3 thin films behaved a strong quantum confinement effect and direct band-gap energy of 1.69 eV when compared with that of bulk Bi_2S_3 [43], which were

weakened by crystal growth. Moreover, the intensity of the absorption peaks decreased after annealing, which may be responsible for high reflectivity of the annealed thin films that had a bright surface as same as metals, as seen in the insert of Fig. 5.

Figure 6 shows dark and light current–voltage characteristics of 6-cycle deposited Bi_2S_3 thin films before and after annealing at 200, 300, 400 °C in a photoelectrochemical cell using 0.25 M Na_2S/0.25 M Na_2SO_3 as electrolytes, platinum plate as counter electrode and Ag/AgCl as reference electrode. The LSV curves of both dark and illumination show that forward bias current density increases with increase of annealing temperature, and current density onset takes place at lower voltages after annealing. The result should be attributed to the increase of
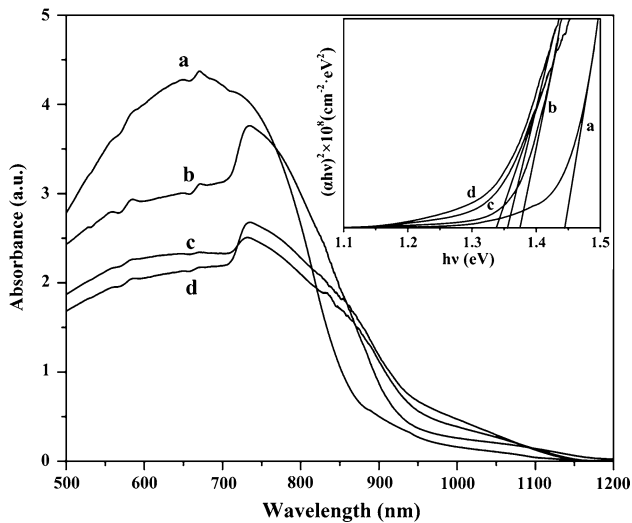
Fig. 10 Optical absorption spectra of the Bi_2S_3 thin films with dip-cycle numbers of *a* 2, *b* 4, *c* 6, *d* 8 and then annealed at 300 °C, and the inset is corresponding $(\alpha h v)^2$–$h v$ curves

recombination in depletion region with the increase of grain size caused by annealing [44]. All the samples exhibited the photo-enhancement effect for the positive potentials under illumination, and the photocurrent density ($I_{ph} = I_{illumination} - I_{darkness}$) values rose with increase of annealing temperature. The as-deposited thin film has

photocurrent density of 2.24 mA/cm^2 at bias of 0.5 V vs. Ag/AgCl, and the thin film annealed at 300 °C showed the highest photocurrent density, about 4.23 mA/cm^2 at bias of 0.5 V, which was higher than that of the previous report [14, 44]. The result indicates that annealing can further improve photo-response of the Bi_2S_3 thin films, which may be attributed to decrease of defects in film structure, and then suppression to recombination of the photon-generated electron–hole pairs, thus leading to a higher photocurrent by annealing. At 400 °C, the behavior of photocurrent response is similar to that at 300 °C.

3.3 Film deposition with dip-cycle numbers

Surface morphologies and cross sections of the Bi_2S_3 thin films with different cycle numbers of 2, 4, 6 and 8, respectively, and then annealed at 300 °C are shown in Fig. 7a–d. It is seen that the four Bi_2S_3 films have similar uniform and densely packed surface morphologies but crystal size becomes lager with different cycle numbers. The film thickness measured by the cross sectional images is about 85, 165, 240 and 320 nm, respectively for dip-cycle number of 2, 4, 6 and 8. In addition, AFM probe scanning was performed to measure the thickness of Bi_2S_3 thin films deposited on slide glass substrates. The thickness of the Bi_2S_3 thin films was examined by scratching dent

Fig. 11 Dark and light current–voltage characteristics of Bi_2S_3 thin films deposited with different dip-cycles: **a** 2 cycles, **b** 4 cycles, **c** 6 cycles and **d** 8 cycles
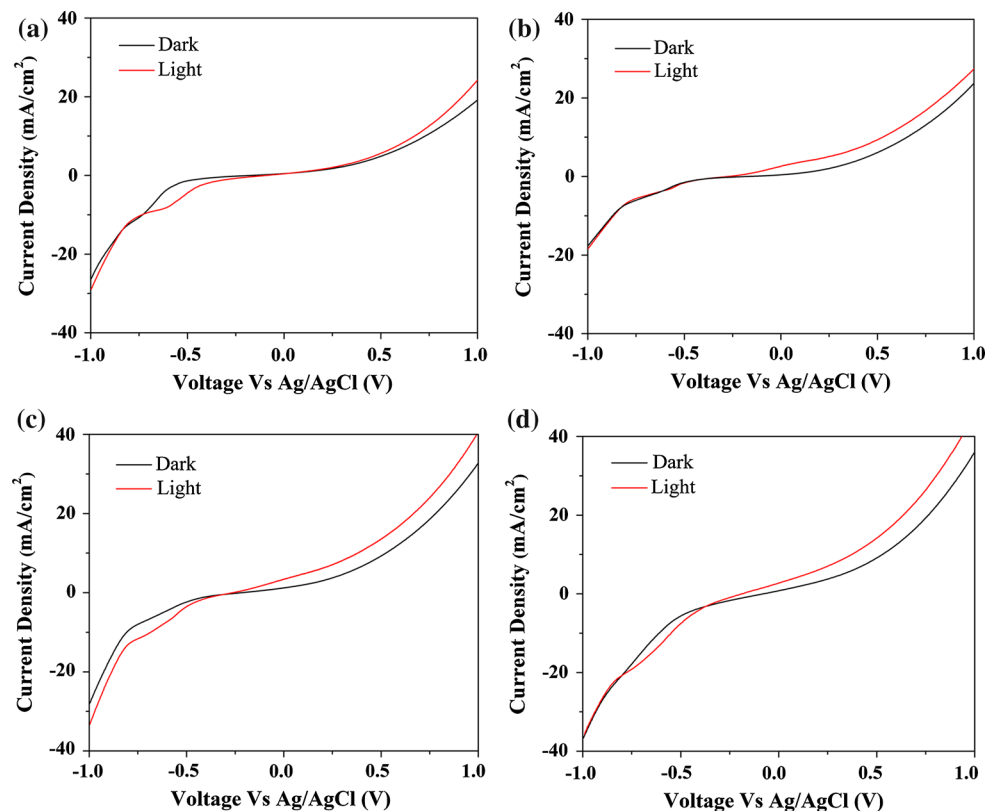
lines on the film surfaces and then scanning film surfaces cross the dent lines. The AFM results are shown Fig. 8. The film thickness is about 78, 161, 232 and 313 nm, respectively, for dip-cycle number of 2, 4, 6 and 8, which is basically consistent with that of the cross sectional SEM image observation above. So, it is concluded that the average deposition rate of film thickness is about 40 nm per deposition cycle. Furthermore, surface roughness of the Bi_2S_3 thin films deposited with 2, 4, 6 and 8 cycle numbers and then annealed at 300 °C was measured by AFM, as shown in Fig. 9. The three-dimensional AFM images show that surface roughness becomes small with increase of deposition cycle numbers. The calculated value of surface roughness by AFM software is 19.8, 14.1, 13.2 and 12.1 nm, respectively, for 2, 4, 6 and 8 deposition cycles (Fig. 9e), showing a self-perfect improvement to surface roughness with increase of deposition cycle numbers. The result is also consistent with the SEM observation above.

Figure 10 is absorption spectra of the Bi_2S_3 thin films deposited with dip-cycle numbers of 2, 4, 6 and 8, respectively. A redshift of absorption edges is observed with increase of cycle numbers. The optical band-gap energies calculated by the Tauc' equation are 1.44, 1.37, 1.36 and 1.33 eV, respectively, for the Bi_2S_3 thin films with 2, 4, 6 and 8 deposition cycles, as shown in inset in Fig. 10. The band-gap values increase slightly from 1.37 to 1.44 eV with decrease of film thickness, which may be related with the small crystal size of Bi_2S_3 thin films with less deposition cycles.

Figure 11 shows the current–voltage (I–V) characteristics in dark and under illumination for the Bi_2S_3 thin films deposited with dip-cycle numbers of 2, 4, 6 and 8, respectively. The LSV curves in dark shows that the forward bias current density increases with increase of film thickness. The photocurrent density are 0.75, 3.27, 4.23 and 5.03 mA/cm^2 under a bias of 0.5 V vs. Ag/AgCl, respectively, for the Bi_2S_3 films with 2, 4, 6 and 8 dip-cycles, which may be due to high thickness decrease defect structure of Bi_2S_3 films.

4 Conclusion

Uniform, smooth and densely packed Bi_2S_3 thin films could be prepared at room temperature by an in situ solution chemical reaction using bismuth nitrate as precursor in a form of thin solid film which was reacted with ammonium sulfide ethanol solution. The as-deposited Bi_2S_3 thin films were almost amorphous phase, and crystallized to orthorhombic structure accompanying with crystal growth by annealing at Ar atmosphere. The in situ solution chemical deposition had a self-improvement to grow smooth and uniform with increase of deposition cycle numbers. The average deposition rate in film thickness was about 40 nm per cycle, showing a high time-efficiency process. The in situ deposited Bi_2S_3 thin films had wide light absorption in the visible region. The photocurrent density were 2.24 and 5.03 mA/cm^2, respectively for the 6 cycle deposited Bi_2S_3 thin films and the 8 cycle thin film annealed at 300 °C.

References

1. Q.J. Guo, S.J. Kim, M. Kar, W.N. Shafarman, R.W. Birkmire, E.A. Stach, R. Agrawal, H.W. Hillhouse, Nano Lett. **8**, 2982 (2008)
2. J.N. Coleman, M. Lotya, A. O'Neill, V. Nicolosi, Science **331**, 568 (2011)
3. L.P. Liu, J. Hensel, R.C. Fitzmorris, Y.D. Li, J.Z. Zhang, J. Phys. Chem. Lett. **1**, 155 (2010)
4. J. Li, Y.J. Lu, Q. Ye, M. Cinke, J. Han, M. Meyyappan, Nano Lett. **3**, 929 (2003)
5. D. Tiwari, T.K. Chaudhuri, T. Shripathi, U. Deshpande, V.G. Sathe, J. Mater. Sci.: Mater. Electron. **25**, 3687 (2014)
6. K.C. Preetha, T.L. Remadevi, J. Mater. Sci.: Mater. Electron. **25**, 1783 (2014)
7. M. Solís, M.E. Rincón, J.C. Calva, G. Alvarado, Electrochim. Acta **112**, 159 (2013)
8. E. Pineda, M.E. Nicho, P.K. Nair, H.L. Hu, Sol. Energy **86**, 1017 (2012)
9. L. Shi, D. Gu, W. Li, L. Han, H. Wei, B. Tu, R.C. Che, J. Alloys Compd. **509**, 9382 (2011)
10. S. Mahmoud, A.H. Eid, H. Omar, Fizika A **6**, 111 (1997)
11. H.H. Huang, J. Chen, Y.Z. Meng, X.Q. Yang, Mi.Z. Zhang, Y. Yu, Z.Y. Ma, Y.D. Zhao, Mater. Res. Bull. **48**, 3800 (2013)
12. L.M. Peter, J. Electroanal. Chem. **98**, 49 (1979)
13. D.J. Desale, S. Shaikh, F. Siddiqui, R. Birajdar, R. Late, A. Ghule, R. Sharm, Composites: Part B **46**, 1 (2013)
14. G. Konstantatos, L. Levina, J. Tang, E.H. Sargent, Nano Lett. **8**, 4002 (2008)
15. R.N. Bhattacharya, P. Pramanik, J. Electrochem. Soc. **129**, 332 (1982)
16. R. Suarez, P.K. Nair, P.V. Kamat, Langmuir **14**, 3236 (1998)
17. J.L. Wu, F. Qin, G. Cheng, H. Li, J.H. Zhang, Y.P. Xie, H.J. Yang, J. Alloys Compd. **509**, 2116 (2011)
18. Z.P. Liu, J.B. Liang, S. Li, S. Peng, Y.T. Qian, Chem. Eur. J **10**, 634 (2004)
19. B. Zhang, X.C. Ye, W.Y. Hou, Y. Zhao, Y. Xie, J. Phys. Chem. B **110**, 8978 (2006)
20. R.C. Jin, G.H. Li, Y.B. Xu, J.S. Liu, G. Chen, Int. J. Hydrog. Energy **39**, 356 (2014)
21. Y.C. Lin, M.W. Lee, J. Electrochem. Soc. **161**, H1–H5 (2014)
22. I. Zumeta-Dubé, V. Ruiz-Ruiz, D. Díaz, S. Rodil-Posadas, A. Zeinert, J. Phys. Chem. C **118**, 11495 (2014)
23. S.B. Rawal, S.D. Sung, S. Moon, Y. Shin, W.I. Lee, Mater. Lett. **82**, 240 (2012)
24. G.T. Yue, J.H. Wu, Y.M. Xiao, J.M. Lin, M.L. Huang, L.Q. Fan, Z. Lan, Sci. China Chem. **56**, 93 (2013)
25. C. Gao, H.L. Shen, L. Sun, Z. Shen, Appl. Surf. Sci. **257**, 7529 (2011)

26. C. Gao, H.L. Shen, L. Sun, Appl. Surf. Sci. **258**, 89 (2011)
27. H.M. Pathan, C.D. Lokhande, Bull. Mater. Sci. **27**, 85 (2004)
28. K. Mageshwari, R. Sathyamoorthy, Mater. Sci. Semicond. Process. **16**, 43 (2013)
29. X.S. Peng, G.W. Meng, J. Zhang, L.X. Zhao, X.F. Wang, Y.W. Wang, L.D. Zhang, J. Phys. D Appl. Phys. **34**, 3224 (2001)
30. A. Jana, C. Bhattacharya, S. Sinha, J. Datta, J. Solid State Electrochem. **13**, 1339 (2009)
31. S.Y. Wang, Y.W. Du, J. Cryst. Growth **236**, 627 (2002)
32. M. Medles, N. Benramdane, A. Bouzidi, A. Nakrela, H. Tabet-Derraz, Z. Kebbab, C. Athieu, B. Khelifa, R. Desfeux, Thin Solid Films **497**, 58 (2006)
33. M.L. Madugu, L. Bowen, O.K. Echendu, I.M. Dharmadasa, J. Mater. Sci.: Mater. Electron. **25**, 3977 (2014)
34. S.H. Mousavi, M.H. Jilavi, T.S. Müller, P.W. Oliveira, J. Mater. Sci.: Mater. Electron. **25**, 2786 (2014)
35. N. Mukherjee, A. Sinha, G.G. Khan, D. Chandra, A. Bhaumik, A. Mondal, Mater. Res. Bull. **46**, 6 (2011)
36. J. Chu, Z.G. Jin, J.X. Yang, Z.L. Hong, J. Am. Ceram. Soc. **95**, 3037 (2012)
37. Y.J. Lu, X. Meng, G.W. Yi, J.H. Jia, J. Colloid Interface Sci. **356**, 726 (2011)
38. A.U. Ubale, A.S. Daryapurkar, R.B. Mankar, R.R. Raut, V.S. Sangawar, C.H. Bhosale, Mater. Chem. Phys. **110**, 180 (2008)
39. J. Chu, Z.G. Jin, W.D. Wang, H. Liu, D.L. Wang, J.X. Yang, Z.L. Hong, J. Alloys Compd. **517**, 54 (2012)
40. J. Chu, Z.G. Jin, S. Cai, J.X. Yang, Z.L. Hong, Thin Solid Films **520**, 1826 (2012)
41. M.E. Rincón, M. Sánchez, P.J. George, A. Sánchez, P.K. Nair, J. Solid State Chem. **136**, 167 (1998)
42. P. Rajalakshmi, R. Oommen, C. Sanjeeviraja, Chalcogenide Lett. **8**, 649 (2011)
43. H. Moreno-Garcíaa, S. Messina, M. Calixto-Rodriguez, H. Martínez, Appl. Surf. Sci. **311**, 729 (2014)
44. R.S. Mane, B.R. Sankapal, C.D. Lokhande, Mater. Chem. Phys. **60**, 196 (1999)